water

MDPI

Article

Synthesis of Na-P1 Zeolite from Municipal Solid Waste Incineration Fly Ash for Efficient Adsorption of Tetracycline from Aqueous Solution

Huiyong Wu [1,2], Tingting Dong [2,*], Zhou Zhang [2], Shengjun Zhang [1], Haiyang Wang [1] and Yue Cheng [1,*]

[1] School of Materials Science and Engineering, Jingdezhen Ceramic University, Jingdezhen 333403, China; huiyongwu@sru.edu.cn (H.W.)
[2] School of Chemistry and Environmental Sciences, Shang Rao Normal University, Shangrao 334001, China
* Correspondence: dongtingting2014@126.com (T.D.); cy_jci@163.com (Y.C.); Tel.: +86-138-7983-9519 (Y.C.)

Abstract

Municipal solid waste incineration (MSWI) fly ash, classified as hazardous waste (HW18) due to the presence of heavy metals and dioxins, necessitates both harmless treatment and resource utilization. In this study, a Na-P1 zeolite adsorbent was synthesised from MSW incineration fly ash using its intrinsic Si and Al sources, supplemented by silica sol and sodium aluminate solution. The synthesised zeolite was employed for the adsorption removal of tetracycline hydrochloride (TCH) from wastewater. Under the optimised conditions (initial TCH concentration of 10 $mg \cdot L^{-1}$, adsorbent dosage of 0.4 $g \cdot L^{-1}$, pH 5.0, temperature 45 °C, and contact time 60 min), a maximum adsorption capacity of 14.8 $mg \cdot g^{-1}$ and a removal efficiency of 59.1% were achieved. Kinetic analysis revealed that the adsorption process followed the pseudo-first-order model (R^2 = 0.975). The Langmuir isotherm provided a better fit than the Freundlich model (R^2 = 0.988), indicating monolayer adsorption on homogeneous sites. Thermodynamic parameters ($\Delta G < 0$, $\Delta H > 0$) confirmed that the adsorption was spontaneous and endothermic, with higher temperatures favoring enhanced TCH adsorption. This work demonstrates the feasibility of converting hazardous MSW incineration fly ash into a value-added Na-P1 zeolite adsorbent with excellent performance for antibiotic wastewater treatment, thereby offering a sustainable strategy for fly ash resource recovery and environmental remediation.

Keywords: fly ash; solid waste management; zeolite; tetracycline; adsorption

check for updates

Academic Editor: Daniela Fighir

Received: 4 September 2025
Revised: 21 October 2025
Accepted: 27 October 2025
Published: 30 October 2025

Citation: Wu, H.; Dong, T.; Zhang, Z.; Zhang, S.; Wang, H.; Cheng, Y. Synthesis of Na-P1 Zeolite from Municipal Solid Waste Incineration Fly Ash for Efficient Adsorption of Tetracycline from Aqueous Solution. *Water* **2025**, *17*, 3118. https://doi.org/10.3390/w17213118

Copyright: © 2025 by the authors. Licensee MDPI, Basel, Switzerland. This article is an open access article distributed under the terms and conditions of the Creative Commons Attribution (CC BY) license (https://creativecommons.org/licenses/by/4.0/).

1. Introduction

The acceleration of urbanization and subsequent improvements in living standards have led to a marked increase in municipal solid waste (MSW) generation, exhibiting a rapid growth trend [1]. Incineration has become the primary disposal method in China due to its advantages of high volume reduction and energy recovery potential [2]. However, this process generates significant quantities of fly ash, accounting for approximately 3–5% (by mass) of the total incinerated waste [3,4]. Fly ash is primarily composed of silica (SiO_2), alumina (Al_2O_3) [5], soluble salts, and heavy metals (e.g., V, Mn, Ni, Hg, Cu, Pb, Cd, Cr, Zn), with potential contamination by highly toxic organic pollutants such as dioxins [6,7]. Consequently, it poses substantial environmental toxicity and leaching risks, and has been classified as hazardous waste (HW18) in China's National Hazardous Waste List [8]. According to the 2025 Statistical Yearbook of Urban and Rural Construction, the annual

generation of MSW incineration fly ash in China reached approximately 18 million metric tons (MT) in 2025.

In recent years, there has been an increasing focus on the synthesis of zeolites from the aluminosilicate components of MSW incineration fly ash as a promising strategy for solid waste valorization [9,10]. Zeolites are crystalline aluminosilicates characterised by a microporous structure, high specific surface area, and excellent thermal stability, and have been widely applied in environmental remediation, catalytic reactions, and ion exchange [11–13]. The zeolites synthesised from fly ash primarily include Na-P1, Na-A, X-type, analcime, and mordenite [14]. These zeolites differ in crystal structure, Si/Al ratio, and cation-exchange capacity, which determine their physicochemical properties and adsorption behavior. Among them, Na-P1 zeolite (GIS topology) exhibits a three-dimensional channel structure, moderate Si/Al ratio, and high cation-exchange capacity, providing it with excellent ion-exchange and adsorption capabilities. In contrast, Na-A and X-type zeolites possess larger pore openings and higher ion-exchange capacity but lower thermal stability, while analcime and mordenite generally form under higher-temperature or low-alkalinity conditions with relatively lower exchange ability. Fly ash-derived zeolites possess abundant and ordered micropores, abundant active surface sites, and negatively charged aluminosilicate frameworks, thereby enabling efficient pollutant capture through physicochemical adsorption mechanisms [9,15]. Among these, Na-P1 zeolite has emerged as a key research focus due to its mild synthesis conditions, high crystallinity, structural stability, and high cation-exchange capacity [16,17]. Moreover, increasing attention has been devoted to employing fly ash-based zeolites as low-cost and efficient adsorbents for environmental purification. Numerous studies have demonstrated their potential for removing heavy metals [18], greenhouse gases [19], dyes, and other organic pollutants from wastewater. Wu et al. [18]. demonstrated that introducing Lewis acid-type bimetallic ions (e.g., Y^{3+} and Zr^{4+}) into fly ash-derived zeolites markedly enhances their adsorption capacity for oxyanion contaminants such as As(V). This enhancement was attributed to the synergistic interaction and structural incorporation of metal ions, which increase active sites and facilitate complexation with the target species. Wei et al. [19]. developed a one-step method to synthesize hierarchically porous NaX zeolites from fly ash, demonstrating that the CTAB/Al_2O_3 ratio can effectively tune mesoporosity and surface area. This structural improvement enhances CO_2 adsorption capacity and cyclic stability by promoting mesopore formation and inhibiting excessive crystal growth. These findings highlight the great potential of converting MSW incineration fly ash into value-added zeolitic materials for wastewater treatment, thereby offering a sustainable pathway for both resource recovery and environmental protection.

Concurrently, the excessive utilization of antibiotics has raised mounting concerns about water contamination, posing substantial threats to sustainable development, human health, and biodiversity [20,21]. Tetracycline hydrochloride (TCH), a prevalent broad-spectrum antibiotic, has been widely utilised in medicine, agriculture, and animal husbandry [22,23]. However, its extensive use, coupled with high structural stability and resistance to biodegradation, leads to long-term environmental persistence and adverse ecosystem impacts [24,25]. The molecular structure of TCH comprises four six-membered rings featuring multiple functional groups (e.g., hydroxyl, amino, and amide groups). The adsorption of TCH on zeolites proceeds via diverse mechanisms, including physical adsorption, chemical adsorption, hydrogen bonding, π–π stacking interactions, and electrostatic interactions [26]. Consequently, the development of fly ash-derived zeolite adsorbents with high adsorption efficiency for TCH removal is critically important.

In this study, transforming municipal solid waste incineration fly ash into functional zeolitic materials presents a promising strategy for both waste valorization and environ-

mental remediation. Zeolites derived from fly ash possess well-developed porosity, high crystallinity, and a tunable framework, which render them suitable for the adsorption of organic contaminants such as tetracycline hydrochloride (TCH) from aqueous solutions. Building on these properties, this study focuses on the hydrothermal synthesis of Na-P1 zeolite from fly ash and its application as an efficient adsorbent for TCH removal. The work aims to systematically evaluate the material's adsorption behaviour, elucidate the underlying kinetics and thermodynamics, and assess the potential of converting hazardous fly ash into a valuable resource for antibiotic-contaminated water treatment, thereby providing both environmental and resource recovery benefits.

2. Materials and Methods

2.1. Reagents and Characterization

The fly ash used in this study was obtained from the air pollution control (APC) system of a municipal solid waste incineration (MSWI) plant in [Jingdezhen, China]. The plant employs a typical grate-firing incineration process operated under excess air at 850–950 °C. The flue gas is treated sequentially by a semi-dry scrubber, bag filter, and induced draft fan. All reagents, including tetracycline hydrochloride (TCH, AR), were purchased from BASF Biotechnology Co., Ltd. (Yuchun, China). Silica sol (SiO_2, AR) was obtained from Kehan Silica Products Co., Ltd. (Linyi, China). Sodium aluminate ($NaAlO_2$, AR) was supplied by Xi'an Tianmao Baoding Biotechnology Co., Ltd. (Xi'an, China). Sodium hydroxide (NaOH, AR) and hydrochloric acid (HCl, AR) were purchased from Tianjin Yufutai Chemical Reagent Co., Ltd. (Tianjian, China). All reagents were used without further purification.

The concentrations of TCH were measured at 357 nm using a UV–Vis spectrophotometer (UV754N, Shanghai, China). The crystalline structure of the samples was analyzed using an X-ray diffractometer (XRD, DX-2700B, Dandong Fangyuan Instrument Co., Ltd., Dandong, China) with Cu Kα radiation (λ = 1.5406 Å) operated at 40 kV and 30 mA over a 2θ range of 5–80°. The surface morphology of the samples was examined using a scanning electron microscope (SEM, EM-30AX, Tianyao Technology Co., Beijing, China) operated at an accelerating voltage of 15 kV.

2.2. Synthesis of Na-P1 Zeolite

Prior to synthesis, fly ash underwent deionization pretreatment by washing with deionised water to remove soluble salts and toxic heavy metals [27]. This pretreatment aimed to improve the structural stability and adsorption performance of the final zeolite. The preparation method was optimised according to the procedure documented by Chen et al. [28]. Briefly, 4 g of pretreated fly ash was combined with 2 g of NaOH. In a parallel step, 3.8 g of sodium aluminate was dissolved in deionised water and mixed with 7 mL of silica sol, resulting in a solid-to-liquid ratio of 1:4 (g:mL). The mixture was stirred at room temperature for 12 h to promote condensation of SiO_4 and AlO_4 tetrahedra and zeolite framework ordering [29]. The aged suspension was then transferred into a Teflon-lined stainless-steel autoclave (100 mL, Shanghai YH Co., China) and subjected to hydrothermal treatment at 120 °C for 24 h under static conditions in an air atmosphere. After cooling, the product was centrifuged and repeatedly washed with deionised water until the supernatant pH reached neutrality. The solid was then vacuum dried for 24 h and ground into a uniform zeolite powder.

2.3. Preparation of Tetracycline Hydrochloride (TCH) Standard Curve Synthesis

A stock solution (1000 mg·L^{-1}) of TCH was prepared by dissolving 500 mg of TCH in deionised water and diluting to 500 mL. The stock was subsequently diluted to prepare standard solutions at 1, 5, 10, 15, 20, 30, and 50 mg·L^{-1}. Absorbance measurements were conducted using a UV-Vis spectrophotometer (λ = 357 nm), and the calibration curve was fitted with Origin software. This yielded a linear regression equation (y = 0.0318x − 0.0022, R^2 = 0.9998), demonstrating excellent linearity over the concentration range (Figure 1).

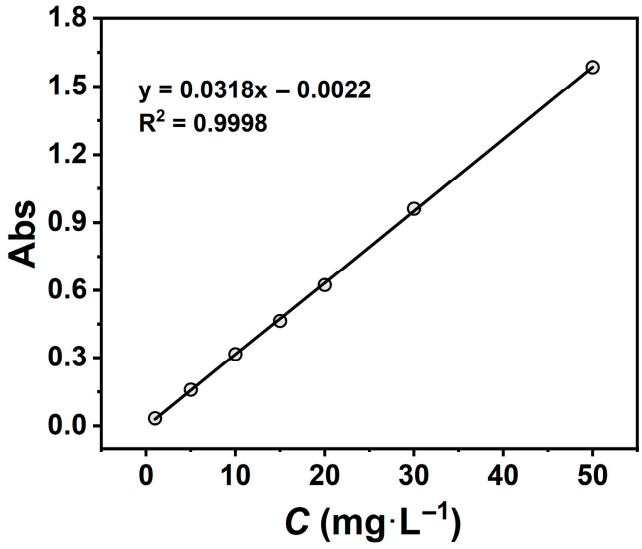


Figure 1. Tetracycline hydrochloride standard curve.

2.4. Batch Adsorption Experiment Preparation

To investigate the effects of operational parameters, batch adsorption experiments were conducted. For adsorbent dosage studies, 50 mL of 10 mg·L^{-1} TCH solution was treated with 20–120 mg of Na-P1 zeolite under shaking at room temperature for 60 min. Initial concentration experiments involved treating 50 mL of TCH solution (5–30 mg·L^{-1}) with the optimal dosage. The pH effect was evaluated by adjusting the pH of 50 mL of 10 mg·L^{-1} TCH to 3, 5, or 7 using 0.1 mol·L^{-1} HCl or NaOH. Contact time experiments involved treating 50 mL of 10 mg·L^{-1} TCH with zeolite for 40–160 min. Temperature studies were conducted at 298, 308, and 318 K using 50 mL of 10 mg·L^{-1} TCH. After adsorption, all samples were centrifuged, and the residual TCH in the supernatant was determined by UV-Vis spectrophotometry. Subsequently, the adsorption capacity and removal efficiency were calculated.

2.5. Adsorption Kinetics

The adsorption kinetics were analysed to evaluate the variation in adsorption capacity with time and to determine the equilibrium time of the system. The experimental data were modelled using the pseudo-first-order and pseudo-second-order kinetic models, expressed as Equations (1) and (2):

$$ln(q_e + q_t) = lnq_e - k_1 t \quad (1)$$

$$\frac{t}{q_t} = \frac{1}{k_2 q_e^2} + \frac{t}{q_e} \quad (2)$$

where q_t (mg·g^{-1}) and q_e (mg·g^{-1}) are adsorption capacities at time t and equilibrium, respectively; k_1 (min^{-1}) and k_2 (g·mg^{-1}·min^{-1}) are rate constants.

2.6. Adsorption Isortherms

Equilibrium adsorption data at varying initial concentrations were modelled with the Langmuir and Freundlich models (see Equations (3) and (4)):

$$\frac{C_e}{q_e} = \frac{1}{K_L q_m} + \frac{C_e}{q_m} \quad (3)$$

$$ln\ q_e = ln\ K_F + \frac{1}{n}\ ln\ C_e \quad (4)$$

where C_e (mg·L^{-1}) is equilibrium concentration, q_m (mg·g^{-1}) is maximum adsorption capacity, K_L (L·mg^{-1}) is Langmuir constant, K_F ((mg·g^{-1}) (L·mg^{-1})$^{1/n}$) is Freundlich constant, n is an empirical parameter that characterizes the favorability of the adsorption process.

2.7. Adsorption Thermodynamics

Thermodynamic experiments were conducted at 298, 308, and 318 K. The distribution coefficient (K_D) was calculated to determine Gibbs free energy (ΔG), enthalpy (ΔH), and entropy (ΔS) changes according to the following Equations (5)–(7):

$$\Delta G = -RTlnK_D \quad (5)$$

$$K_D = \frac{q_e}{C_e} \quad (6)$$

$$lnK_D = -\frac{\Delta H}{RT} + \frac{\Delta S}{R} \quad (7)$$

where R is the gas constant (8.314 J·mol^{-1}·K^{-1}), T is temperature (K), q_e (mg·g^{-1}) is adsorption capacity, and C_e (mg·L^{-1}) is equilibrium concentration.

3. Results and Discussion

3.1. Chemical Composition Analysis of Fly Ash

To evaluate the feasibility of using municipal solid waste incineration (MSWI) fly ash in zeolite synthesis and its impact on material performance, compositional changes in fly ash from the LePing MSWI plant before and after water-washing pretreatment were analysed (Table 1). X-ray fluorescence (XRF) analysis identified the primary constituents of SiO_2, Al_2O_3, CaO, Na_2O, K_2O, and MgO, with CaO being the most abundant. Quantitatively, the contents of CaO, SiO_2, and Al_2O_3 increased from 34.15% (unwashed) to 40.86% (washed), 10.22% to 15.95%, and 3.55% to 5.56%, respectively. This compositional change indicates that water-washing removes soluble salts, thereby enriching the relative proportions of Si and Al—key precursors for zeolite framework formation ([SiO_4] and [AlO_4] tetrahedra). Calcium (Ca) acts as a charge-balancing cation and framework modifier, promoting crystal growth and stabilizing the zeolite structure.

Residual trace metals (e.g., Cu, Zn, Pb) in washed fly ash can be incorporated into the zeolite lattice through isomorphous substitution, enabling modulation of surface charge density and acidity to enhance adsorption performance. For instance, Chen et al. [30] synthesised Co-doped NaP zeolite, demonstrating a 2.5-fold increase in pore volume compared to the undoped sample, with Pb(II) removal efficiency achieving 98.8%. Collectively, these results suggest that metal doping optimizes the pore structure and adsorption capacity of zeolites. Thus, trace metals inherent in fly ash may act as dopants during zeolite synthesis, establishing a theoretical basis for the enhanced adsorption observed in this study.

Table 1. Chemical composition of fly ash before and after water-washing.

Composition	Fly Ash Before Washing (%)	Fly Ash After Washing (%)
SiO_2	10.22	15.95
Al_2O_3	3.55	5.56
TFe_2O_3	1.36	2.24
CaO	34.15	40.86
MgO	3.39	5.51
K_2O	5.04	0.62
Na_2O	4.59	1.12
P_2O_5	0.78	1.24
SO_3	6.36	8.53
MnO	0.04	0.07
TiO_2	0.48	0.84
CuO	0.08	0.07
SrO	0.03	0.03
ZnO	0.37	0.86
PbO	0.10	0.13
Cl	10.96	0.76
IL	18.50	15.38

TFe_2O_3: total Fe expressed as Fe_2O_3 equivalent; IL: ignition loss at 950 °C.

3.2. Effect of Zeolite Dosage on Adsorption Performance

The dosage of zeolite is a critical factor affecting adsorption performance, as it determines the availability of adsorption sites and contaminants removal efficiency [31]. To investigate this effect, tetracycline hydrochloride (TCH) adsorption was studied by varying zeolite dosages. Figure 2a shows that adsorption capacity ($mg \cdot g^{-1}$) decreased significantly with increasing zeolite dosage, from 13.8 to 3.7 $mg \cdot g^{-1}$. This trend arises from the fixed total TCH mass in solution; at higher doses, unsaturated sites remain available, reducing adsorbent utilization. Conversely, Figure 2b demonstrates that removal efficiency increased directly with zeolite dosage, rising from 55.3% to 87.8% at 20–120 mg. Higher dosages provide more accessible adsorption sites, enhancing contaminant removal.

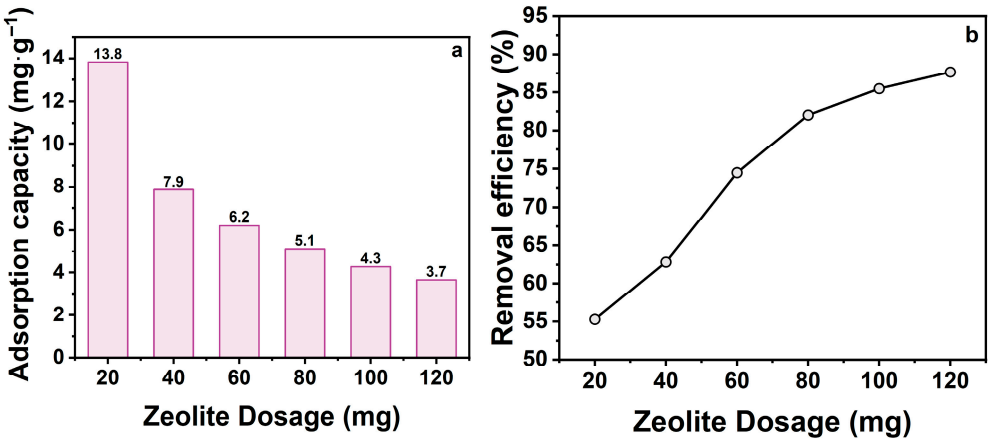


Figure 2. (**a**) Effect of zeolite dosage on adsorption capacity; (**b**) Effect of zeolite dosage on removal efficiency. (C_{TCH} = 10 $mg \cdot L^{-1}$, t = 60 min, pH = 7).

Balancing utilization efficiency and removal rate is essential for cost-effectiveness. Based on these results, 20 mg (0.4 $g \cdot L^{-1}$) was selected as optimal, representing a trade-off between economic feasibility and adsorption performance.

3.3. Adsorption Kinetics and Thermodynamics

The initial concentration of tetracycline hydrochloride (TCH) influences the mass transfer driving force and final removal efficiency. To investigate this effect, zeolite adsorption performance was systematically studied under different initial TCH concentrations (Figure 3). Figure 3a shows that with constant zeolite dose, contact time, and temperature, adsorption capacity was highly dependent on initial concentration. The adsorption capacity increased from 5 to 20 mg·L^{-1} but plateaued at higher concentrations. This suggests that elevated concentrations enhance mass transfer, promoting TCH diffusion into zeolite pores. However, once the available adsorption sites on the surface and within the pore channels were saturated, further adsorption capacity increases were limited, demonstrating typical saturation behaviour. Figure 3b reveals that removal efficiency declined from 55.3% to 38.0% as the initial concentration increased from 10 to 30 mg·L^{-1}. This decline is attributed to the fixed zeolite dosage: higher TCH concentrations increase the quantity of molecules available for adsorption, but the limited active sites become progressively occupied, reducing overall removal efficiency.

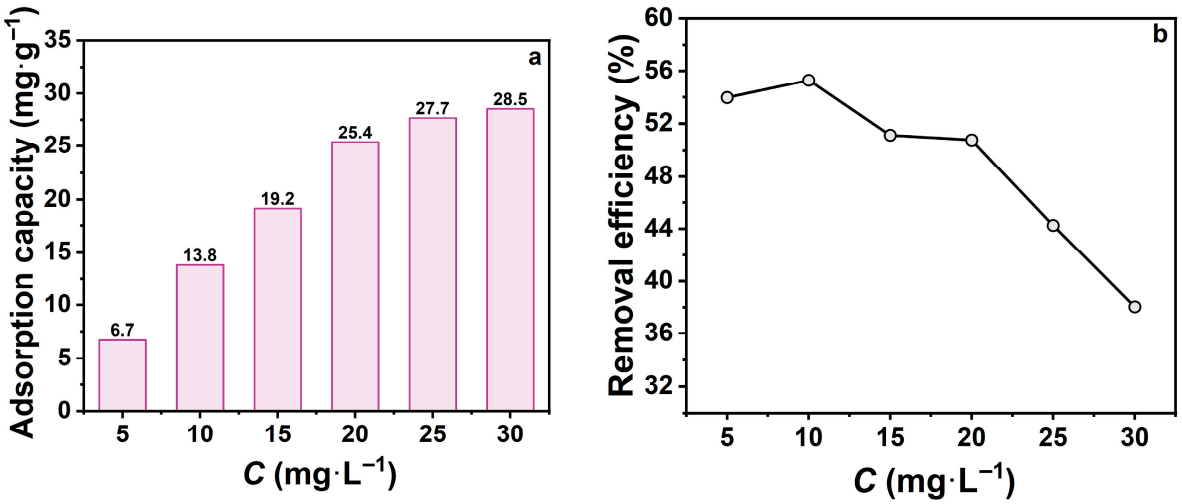


Figure 3. (**a**) Effect of initial TCH concentration on adsorption capacity; (**b**) Effect of initial TCH concentration on removal efficiency. (m_z = 20 mg, t = 60 min, pH = 7).

In summary, lower initial concentrations favor higher removal efficiency, while higher initial concentrations increase adsorption capacity but reduce removal efficiency. Therefore, an initial TCH concentration of 10 mg·L^{-1} was chosen as optimal condition for subsequent experiments.

Contact time is a pivotal kinetic parameter for evaluating TCH adsorption onto zeolite, reflecting the transition from rapid to equilibrium adsorption stages. In this study, contact times of 40, 60, 80, 100, 120, 140, and 160 min were systematically examined (Figure 4) Both adsorption capacity and removal efficiency increased with contact time. Within the first 60 min, adsorption capacity increased rapidly from 11.3 to 14.0 mg·g^{-1}, while removal efficiency rose from 45.2% to 58.1%. This indicates that abundant active sites on the zeolite surface and within pores facilitated rapid TCH diffusion and occupation. Beyond 80 min, growth rates slowed as available sites decreased, approaching dynamic equilibrium. Notably, after 140 min, both metrics stabilised, suggesting saturation of most adsorption sites and minimal performance gain from extended contact. While prolonged contact enhances adsorption, its benefits diminish post-equilibrium, potentially increasing energy costs. Therefore, a contact time of 60 min was chosen as optimal for subsequent experiments.

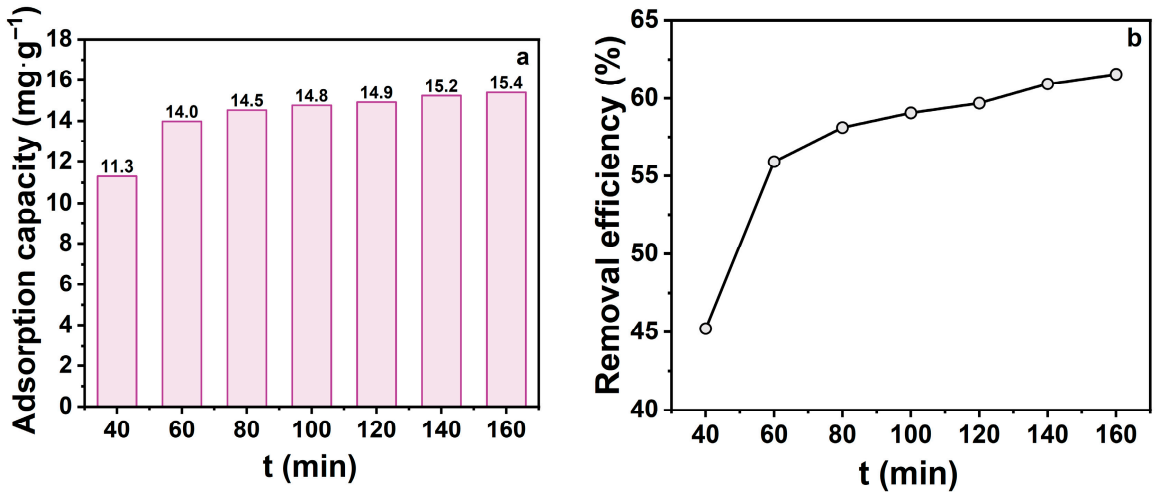


Figure 4. (**a**) Effect of shaking time on adsorption capacity; (**b**) Effect of shaking time on removal efficiency. (C_{TCH} = 10 mg·L^{-1}, m_z = 20 mg, pH = 7).

3.4. Effect of pH on Adsorption Performance

Solution pH is a pivotal factor influencing the adsorption, as it determines the adsorbent's surface charge and affects the structural stability of TCH molecules. In alkaline environments, TCH undergoes cleavage of the C-ring, forming inactive lactone structures and altering its physicochemical properties, which reduces adsorption capacity. These pH-induced alterations directly influence TCH-zeolite interactions. To investigate this effect, adsorption experiments were conducted at pH 3, 5, and 7 (Figure 5). Na-P1 zeolite showed optimal adsorption capacity at pH 5. Deviation toward acidic or alkaline conditions reduced efficiency, with greater decline in alkaline environments.

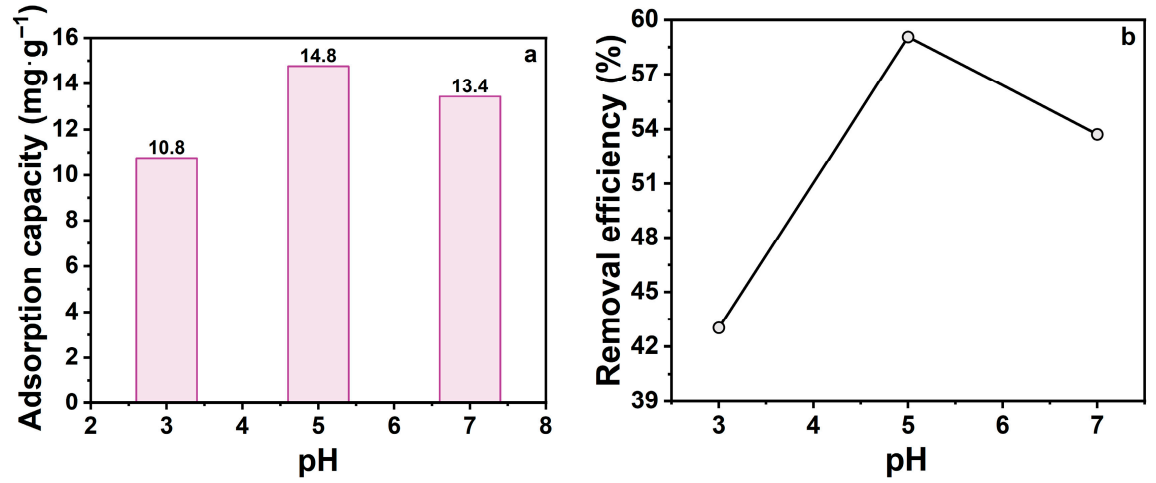


Figure 5. (**a**) Effect of pH on the adsorption capacity; (**b**) Effect of pH on the removal efficiency. (C_{TCH} = 10 mg·L^{-1}, m_z = 20 mg, t = 60 min).

Previous studies demonstrated that this behavior is highly pH-dependent. At low pH, TCH predominantly exists in cationic form (TCH^+), causing electrostatic repulsion with positively charged Na-P1 sites and thus suppressing adsorption. As pH increases, TCH transforms into neutral or anionic species (TCH^0/TCH^-), which can interact with negatively charged sites on the zeolite through electrostatic attraction or hydrogen bonding with the zeolite surface. Additionally, the surface functional groups of Na-P1 exhibit pH-dependent charge properties, further modulating adsorption. Under neutral to mildly alkaline conditions, TCH dissociation favors the formation of species that can be effectively

adsorbed. However, strongly alkaline environments can induce irreversible degradation reactions such as ring-opening or deamidation, generating byproducts with low adsorption affinity. These observations highlight that the adsorption process is governed by the interplay of TCH speciation, surface charge of Na-P1, and chemical stability of TCH under different pH conditions, providing a mechanistic explanation for the experimental trends observed in this study.

In summary, Na-P1 adsorption performance is highly pH-sensitive. These findings support pH adjustment as a key optimization strategy for water treatment applications. Subsequent experiments were performed at pH 5 (optimal conditions).

3.5. Adsorption Kinetics Analysis

To identify the rate-controlling mechanism, TCH adsorption onto Na-P1 was analysed using pseudo-first-order and pseudo-second-order kinetic models. A 50 mL TCH solution (10 mg·L^{-1}) was mixed with 20 mg Na-P1, sealed, labeled, and incubated in a thermostatic shaker (25 °C). Kinetic data are presented in Figure 6 and Table 2.

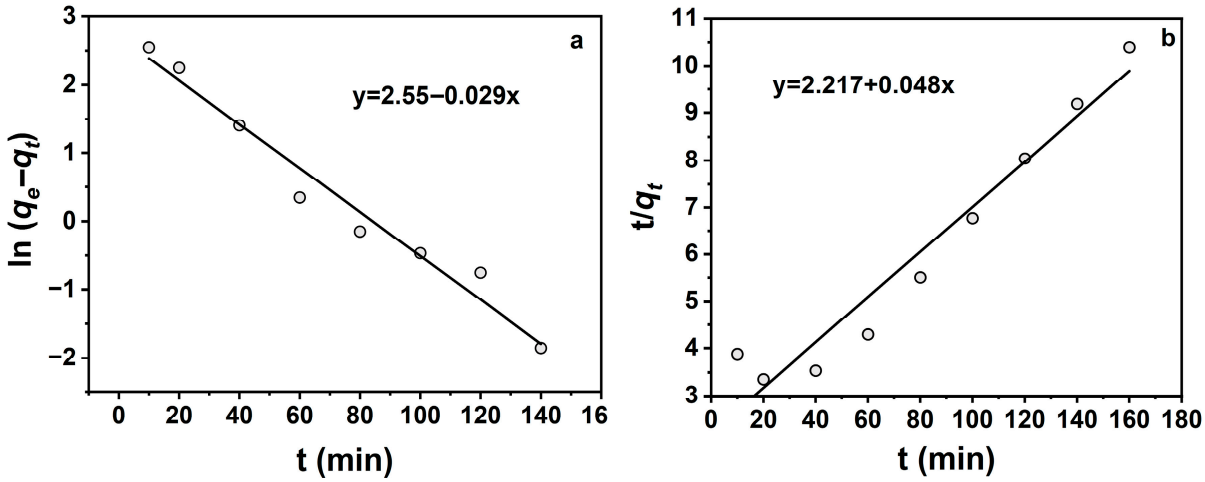


Figure 6. (**a**) Pseudo-first-order kinetic fitting curve; (**b**) Pseudo-second-order kinetic fitting curve.

Table 2. Adsorption kinetic model fitting parameters.

Pseudo-First-Order			Pseudo-Second-Order		
k_1 (min^{-1})	q_e	R^2	k_2 (g·mg^{-1}·min^{-1})	q_e	R^2
0.03	12.8	0.97	0.001	20.9	0.94

Figure 6 shows that adsorption was better described by the pseudo-first-order model (R^2 = 0.97), indicating predominant pseudo-first-order kinetics. Table 2 confirms that the pseudo-first-order model yielded a higher correlation coefficient (R^2 = 0.97) compared to the pseudo-second-order model (R^2 = 0.94), suggesting that the pseudo-first-order model provides a slightly better overall fit to the experimental data.

However, the calculated equilibrium adsorption capacity (q_e) from the pseudo-second-order model (20.85 mg·g^{-1}) was higher than both the pseudo-first-order model (12.8 mg·g^{-1}) and the experimentally observed maximum adsorption capacity (15.8 mg·g^{-1}). This suggests that while the pseudo-second-order model may overestimate the equilibrium capacity, it still captures the chemisorption tendency of the system, which involves electron sharing or exchange between the adsorbent and adsorbate. In contrast, the pseudo-first-order model, which predicts a lower q_e, typically represents physisorption-dominated processes driven primarily by surface adsorption kinetics. Therefore, the adsorption process likely involves

a combination of mechanisms, with both physisorption and chemisorption contributing to the observed behavior.

These findings indicate that the TCH adsorption on Na-P1 follows pseudo-first-order kinetics, with rate-controlling steps likely involving film diffusion or intraparticle diffusion. This diffusion-controlled mechanism enables rapid equilibrium attainment, highlighting Na-P1's fast kinetic profile for TCH removal.

To further investigate the effect of initial TCH concentration on Na-P1 equilibrium adsorption capacity, data were fitted using Langmuir and Freundlich isotherm models (Table 3, Figure 7). The linear fitting results show that the Langmuir model exhibited a higher correlation coefficient (R^2 = 0.98) than the Freundlich model (R^2 = 0.94), indicating that the Langmuir model provides a better representation of the experimental data. The maximum adsorption capacity (q_m) and Langmuir constant (K_L) were calculated to be 50.8 mg·g^{-1} and 0.08 L·mg^{-1}, respectively, confirming that the adsorption tends to occur on a homogeneous surface with uniform active sites. In contrast, the Freundlich model yielded K_F = 4.36 and n = 1.42, suggesting a favorable adsorption process and a moderate interaction strength between TCH and the adsorbent surface. However, the relatively lower R^2 value indicates that the Freundlich model is less suitable for describing the adsorption behavior in this system. Therefore, the Langmuir model is more appropriate for describing TCH adsorption on Na-P1, implying that monolayer adsorption is the dominant mechanism.

Table 3. Na-P1 molecular sieve adsorption isotherm model fitting parameters for TCH.

Langmuir Model			**Freundlich Model**		
K_L	q_m	R^2	K_F	n	R^2
0.08	50.8	0.98	4.36	1.42	0.94

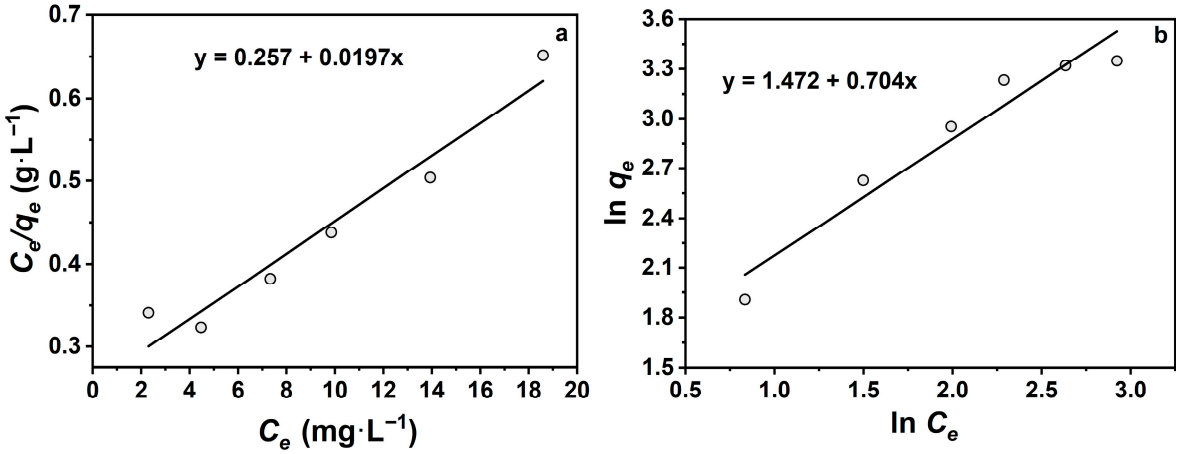


Figure 7. (**a**) Langmuir model adsorption isotherm fitting curve; (**b**) Freundlich model adsorption isotherm fitting curve.

3.6. Thermodynamics Analysis of Adsorption

This study investigated temperature effects on adsorption using thermodynamics. Adsorption tests were conducted at 298 K, 308 K, and 318 K under identical conditions, with results shown in Figure 8. Na-P1 adsorption capacity increased slightly with temperature: 12.3 mg·g^{-1} at 298 K, 13.0 mg·g^{-1} at 308 K, and 14.0 mg·g^{-1} at 318 K. This indicates temperature-dependent adsorption enhancement, suggesting an endothermic process. Elevated temperatures enhanced molecular diffusion, increased kinetic energy, and activated surface sites, promoting TCH penetration into zeolite channels and binding to active sites. Additionally, higher temperatures modified TCH dissociation in solution, facilitating migration and improving adsorption capacity.

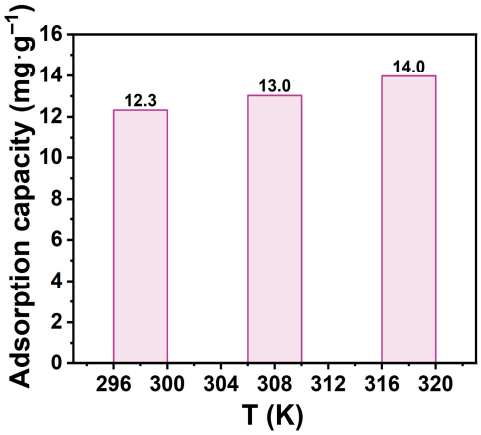


Figure 8. Effect of temperature on the adsorption capacity. (C_{TCH} = 10 mg·L^{-1}, m_z = 20 mg, t = 60 min, pH = 7).

To further elucidate temperature effects, thermodynamic parameters (ΔG, ΔH, ΔS) for TCH adsorption onto Na-P1 zeolite were calculated, with results shown in Figure 9 and Table 4. All ΔG values were negative, and the absolute values increased with increasing temperature, indicating a thermodynamically favorable and temperature-enhanced process. Positive ΔH confirmed endothermicity, while positive ΔS reflected increased system disorder. This entropy rise likely results from solvent release during TCH desolvation and diffusion toward the adsorbent surface. It can thus be concluded that the adsorption process is spontaneous, endothermic, and entropy-driven, suggesting physical/chemical interactions between TCH and Na-P1 zeolite. Adsorption capacity increased slightly with temperature, demonstrating thermal responsiveness. These findings highlight temperature as a critical parameter for optimizing TCH removal efficiency.

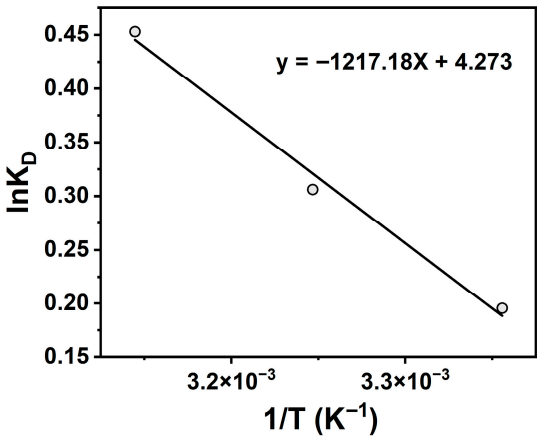


Figure 9. Van't Hoff equation linear fit of lnK_D and 1/T.

Table 4. Thermodynamic parameters of tetracycline hydrochloride adsorption on Na-P1 molecular sieve.

T (K)	ΔG (kJ·mol^{-1})	ΔS (J·mol^{-1}·K^{-1})	ΔH (kJ·mol^{-1})
298	−0.48457		
308	−0.78419	35.525	10.120
318	−1.19753		

3.7. Na-P1 Zeolite: Characterization and Analysis

The phase composition and microstructure of the synthesised Na-P1 zeolite were systematically characterised using XRD and SEM. As demonstrated in Figure 10, the

XRD pattern exhibited distinct diffraction peaks at 2θ = 13.2°, 23.1°, 26.0°, 30.9°, 31.9°, 34.1°, and 35.6°, matching the standard Na-P1 zeolite reference (PDF#39-0219). These results confirm the successful synthesis of Na-P1 zeolite under the applied hydrothermal conditions. Weak-to-moderate intensity reflections at 2θ = 29.4° and 36.0° were attributed to calcite ($CaCO_3$, PDF#05-0586). This finding indicates the presence of minor $CaCO_3$ residues [32]. These residues likely originated from unreacted calcium species in raw fly ash or precipitation byproducts during synthesis. The Na-P1 phase showed strong reflections in the low-angle region (10–35°), indicating high crystallinity and ordered structure. The sharp decline in signal intensity at higher angles (40–80°) aligns with typical zeolite crystallographic characteristics.

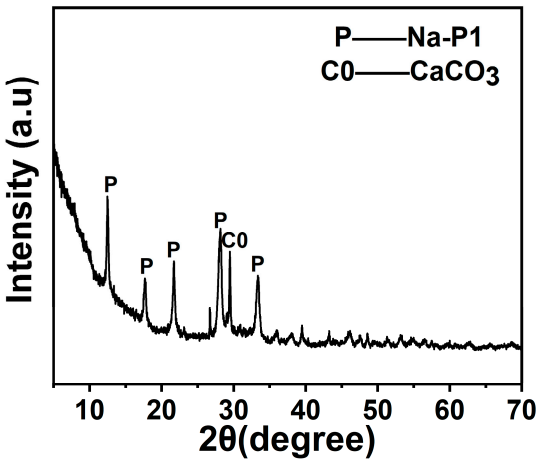


Figure 10. T XRD pattern of Na-P1 zeolite.

The SEM image (Figure 11) corroborates XRD findings. Particles exhibit a regular plate-like morphology, with intergrown fibrous/columnar crystals in specific regions. The zeolite structure is porous and loose, with uniformly distributed crystal grains, indicating high Na-P1 crystallinity [16]. These morphological traits align with literature reports on Na-P1 [33]. However, dense blocky agglomerates with smooth surfaces and poorly developed crystal facets are observed in some regions. This morphology likely arises from high CaO content in fly ash, where free Ca^{2+} forms $CaCO_3$ precipitates in alkaline conditions. These precipitates inhibit dissolution of silicate and aluminate species, impeding complete zeolite framework reconstruction. Collectively, XRD and SEM analyses confirm successful synthesis of high-crystallinity Na-P1 zeolite from water-washed MSWI fly ash. Minor $CaCO_3$ coexistence highlights calcium influence on precursor dissolution, providing insights into crystallization and purity control.

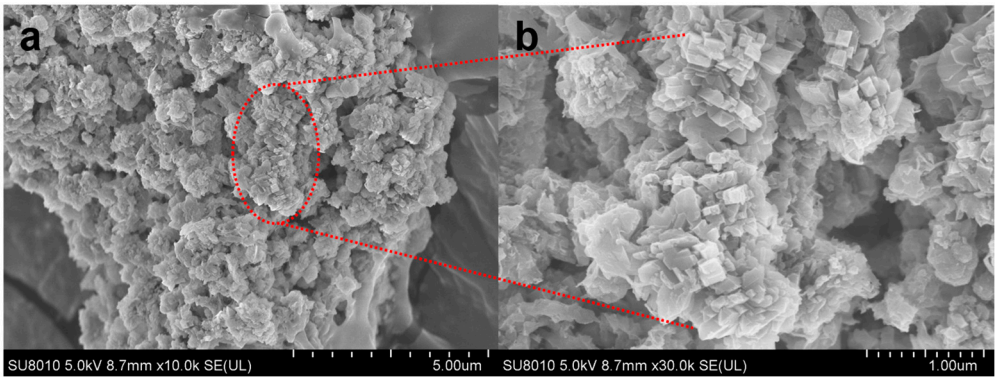


Figure 11. (**a**) SEM characterization of Na-P1 zeolite; (**b**) Magnified view of the selected region.

4. Conclusions

This study utilised municipal solid waste incineration (MSWI) fly ash as the primary raw material, with silica sol and sodium aluminate providing additional silicon and aluminum sources. Using a hydrothermal method, Na-P1 zeolite was successfully synthesised. XRD and SEM analyses confirmed that the zeolite exhibited high crystallinity, ordered structure, and abundant porosity. Single-factor experiments systematically evaluated adsorption parameters, identifying optimal conditions: 0.4 $g \cdot L^{-1}$ dosage, pH 5, and 60 min shaking time yielded maximum tetracycline hydrochloride removal. Mechanistic investigations revealed an endothermic process with enhanced adsorption at higher temperatures. Kinetics followed a pseudo-first-order model, suggesting film diffusion as the rate-limiting step, while equilibrium data fit the Langmuir isotherm, indicating monolayer adsorption. Thermodynamic parameters confirmed spontaneous, endothermic adsorption with good thermal stability. This work achieved two objectives: 1) valorizing MSWI fly ash with significant economic potential, and 2) developing a high-performance zeolite adsorbent for antibiotic removal. These findings offer theoretical guidance and practical references for designing environmental materials and remediating antibiotic pollution.

Author Contributions: Conceptualization, formal analysis, methodology, and writing—original draft preparation, H.W. (Huiyong Wu); funding acquisition and supervision, T.D. and Y.C.; investigation, Z.Z.; formal analysis, S.Z.; writing—review and editing, data curation, H.W. (Haiyang Wang). All authors have read and agreed to the published version of the manuscript.

Funding: This research was funded by the Education Department of Jiangxi Province, China [grant number GJJ2401705, GJJ190892 and GJJ201719] and the Jingdezhen Municipal Science and Technology Project, China [grant number 2023GY005].

Data Availability Statement: The original contributions presented in this study are included in the article. Further inquiries can be directed to the corresponding authors.

Conflicts of Interest: All authors declare that the research was conducted in the absence of any commercial or financial relationships that could be construed as potential conflicts of interest.

References

1. Jara-Echeverría, H.D.; Sánchez-Redondo, I.; Rivas-Seijas, J.A.; Nieto-Márquez, A.; Díaz-López, J.A.; Atanes-Sánchez, E. Two-stage separation-immobilization method for municipal solid waste incineration fly ash treatment. *Chem. Eng. Res. Des.* **2025**, *219*, 272–282. [CrossRef]
2. He, H.; Gao, Y.; Yu, J.; Zhang, W.; Shen, X.; Zhang, M. Municipal solid waste incineration fly ash as activator for ground granulated blast-furnace slag: Hydration behavior and stabilization/solidification effectiveness. *Case Stud. Constr. Mater.* **2025**, *23*, e05177. [CrossRef]
3. Aghabeyk, F.; Chen, B.; Brito van Zijl, M.; Ye, G. Physicochemical characterization and resource recovery potential of hazardous municipal solid waste incineration (MSWI) fly ash and air pollution control (APC) residues in the Netherlands. *J. Environ. Manag.* **2025**, *384*, 125579. [CrossRef]
4. Shen, X.; He, H.; He, C.; Li, B.; Luo, W.; Ren, P. Low-carbon blended cement containing wet carbonated municipal solid waste incineration fly ash and mechanically activated coal fly ash. *Case Stud. Constr. Mater.* **2024**, *21*, e03671. [CrossRef]
5. Yang, D.; Kow, K.-W.; Wang, W.; Meredith, W.; Zhang, G.; Mao, Y.; Xu, M. Co-treatment of municipal solid waste incineration fly ash and alumina-/silica-containing waste: A critical review. *J. Hazard. Mater.* **2024**, *479*, 135677. [CrossRef] [PubMed]
6. Shen, H.; Liu, B.; Lou, B.; Zhang, J.; Zhang, X.; Shen, H.; Liu, J.; Zhang, S. Separation of heavy metals from municipal solid waste incineration fly ash: A review. *Ecotoxicol. Environ. Saf.* **2025**, *299*, 118363. [CrossRef] [PubMed]
7. Soylu, E.; Lode, S.; Silva, C.M.; Simavik, K.R.; Ekstrøm, K.E.; Johansson, I.; Sørensen, B.E.; Kowalczuk, P.B.; Tranell, G. Comprehensive characterization of solid waste incineration fly ash before and after salt washing: Evaluating analytical methods for sustainable waste management. *Resour. Conserv. Recycl. Adv.* **2025**, *27*, 200268. [CrossRef]
8. Vele, A.M.; Galisteo, F.C.; Atanes-Sánchez, E.; Nieto-Márquez, A.; Martín de Vidales, M.J. Sustainable management of municipal solid waste incineration fly ash: A life cycle assessment based review of treatment and valorization pathways. *J. Hazard. Mater. Adv.* **2025**, *19*, 100817. [CrossRef]

9. Yang, D.; Kow, K.-W.; Meredith, W.; Peng, Y.; Wang, L.; Li, X.; Zhang, G.; Zhang, J.; Chen, G.; Li, J.; et al. Green synthesis of NaP1 zeolite from MSWI fly ash and silica-rich solid waste with superior Cu(II) removal efficiency. *Chem. Eng. J.* **2025**, *522*, 167475. [CrossRef]
10. Quddus, M.S.; Saha, M.; Hasanuzzaman, M.; Sharmin, N.; Bashar, M.S. Low energy synthesis of crystalline mesoporous aluminosilicate consisting of Na-P1 zeolite derived from coal fly ash. *Clean. Mater.* **2024**, *12*, 100247. [CrossRef]
11. Qin, B.; Zhang, T.; Liu, Y.; Chen, Z.; Gao, H.; Du, Y.; Hou, S.; Zheng, J. Design and synthesis of core-shell Y zeolite: A tandem microreactor facilitating efficient and targeted conversion of heavy oil macromolecules. *Mater. Today Sustain.* **2025**, *31*, 101165. [CrossRef]
12. Karantoumanis, F.; Tsamos, P.; Noli, F. Exploration of sorption properties of Greek zeolites for Cs- and U-removal from aqueous solutions. *Appl. Radiat. Isot.* **2025**, *225*, 111995. [CrossRef]
13. Ibsaine, F.; Dionne, J.; Tran, L.H.; Coudert, L.; Pasquier, L.-C.; Blais, J.-F. Application of aluminosilicate residue-based zeolite from lithium extraction in water treatment. *Microporous Mesoporous Mater.* **2025**, *381*, 113370. [CrossRef]
14. Gui, T.; Wu, X.; Li, Y.; Tan, J.; Wang, X.; Zhang, F.; Chen, X.; Kita, H. Reproducible scale-up of high-selectivity 80-cm-long NaA zeolite membranes via green gel-less conversion method for dehydration of ethanol. *Mater. Des.* **2025**, *257*, 114524. [CrossRef]
15. Prajaputra, V.; Abidin, Z.; Budiarti, S.; Suryaningtyas, D.T. Synergistic effect of adsorption and Fenton-like oxidation processes for Methylene blue removal using Na-P1 zeolite prepared from pumice. *Desalination Water Treat.* **2021**, *218*, 401–408. [CrossRef]
16. Meftah, M.; Oueslati, W.; Chorfi, N.; Ben Haj Amara, A. Effect of the raw material type and the reaction time on the synthesis of halloysite based Zeolite Na-P1. *Results Phys.* **2017**, *7*, 1475–1484. [CrossRef]
17. Duangkham, S.; Pengproh, R.; Thuadaij, P. Facile preparation of zeolite Na–P supported by nanozinc oxide for antibacterials. *Curr. Res. Green Sustain. Chem.* **2025**, *10*, 100459. [CrossRef]
18. Wu, X.; Han, Y.; Yang, L.; Xi, L.; Jia, S.; Chen, K.; Zhang, J.; Bai, H.; Nagasaka, T. Bimetallic ion location and their synergistic effect on arsenic adsorption in fly ash based-modified zeolite: Experimental and simulation approaches. *J. Environ. Chem. Eng.* **2025**, *13*, 118196. [CrossRef]
19. Wei, Y.; Wu, H.; Kong, H.; Miao, Y.; Wang, P. One-step synthesis of hierarchically porous fly ash-based NaX zeolite as assisted by CTAB for low-concentration CO_2 adsorption. *Particuology* **2025**, *97*, 69–79. [CrossRef]
20. Liu, Q.; Mao, Y.; Jiao, Y.; Li, R.; Mian, B.; Li, P.; Lei, J.; Liu, Y. Photoelectrocatalytic coupled chlorine degradation of tetracycline hydrochloride in recirculating aquaculture system (RAS). *Results Chem.* **2025**, *16*, 102340. [CrossRef]
21. Nguyen, S.H.; Tran, M.T. Enzyme-free biosensor utilizing chitosan-capped ZnS doped by Mn nanomaterials for tetracycline hydrochloride detection. *Heliyon* **2024**, *10*, e40340. [CrossRef]
22. Ravichandran, S.; Thanikaivelan, P. Sustainable solar driven photodegradation of ranitidine hydrochloride and tetracycline using Ag_2O-TiO_2/carbon nanocomposite: Mechanistic insights and environmental implications. *Mater. Today Sustain.* **2025**, *31*, 101191. [CrossRef]
23. Lian, J.; Li, W.; Tao, H.; Chen, B.; Lian, J.; Kong, Q.; Li, Q. Octahedral zero-valent copper activated peracetic acid for efficient tetracycline hydrochloride degradation under neutral condition: Theoretical calculation and toxicity evaluation. *Environ. Chem. Ecotoxicol.* **2025**, *7*, 910–923. [CrossRef]
24. Jiao, Y.; Lu, S.; Li, R.; Liu, Q.; Ma, Y.; Fu, F.; Mao, Y.; Liu, Y. Alkali metal salt modulated visible photocatalytic degradation of tetracycline hydrochloride by g-C_3N_4: Degradation pathway, mechanism and toxicity assessment. *Results Chem.* **2025**, *13*, 102047. [CrossRef]
25. Zou, W.; Zhang, M.; Zhang, X.; Zhang, D.; Li, C.; Zhong, L.; Guo, W.; Ngo, H.H. Optimized performance and mechanistic analysis of tetracycline hydrochloride removal using biochar-based alginate composite magnetic beads for peroxymonosulfate activation. *J. Environ. Chem. Eng.* **2025**, *13*, 115742. [CrossRef]
26. Brauer, J.; Fischer, M. Emerging extra-large pore zeolites as adsorbents for antibiotics: A comparative computational study. *Microporous Mesoporous Mater.* **2025**, *398*, 113832. [CrossRef]
27. Han, A.; Wang, R.; Zhang, C.; Wang, H.; Wang, Z. Preparation of Ceramsite from heavy metal contained municipal solid waste incineration fly ash synergistically with Silicon/Aluminum-containing waste. *J. Hazard. Mater. Adv.* **2025**, *18*, 100725. [CrossRef]
28. Chen, Q.; Long, L.; Liu, X.; Jiang, X.; Chi, Y.; Yan, J.; Zhao, X.; Kong, L. Low-toxic zeolite fabricated from municipal solid waste incineration fly ash via microwave-assisted hydrothermal process with fusion pretreatment. *J. Mater. Cycles Waste Manag.* **2020**, *22*, 1196–1207. [CrossRef]
29. Bahmanzadegan, F.; Ghaemi, A. A comprehensive review on novel zeolite-based adsorbents for environmental pollutant. *J. Hazard. Mater. Adv.* **2025**, *17*, 100617. [CrossRef]
30. Chen, Y.; Sun, J.; Han, H.; Wu, X.; Zhang, M.; Zhang, Y.; Deng, J.; Guan, J. Preparation of NaP Zeolite Doped with Cobalt and Its Adsorption Performance for Pb(II). *Bull. Chin. Ceram. Soc.* **2021**, *40*, 653–657. [CrossRef]
31. Aigbe, U.O.; Ukhurebor, K.E.; Onyancha, R.B.; Osibote, O.A.; Darmokoesoemo, H.; Kusuma, H.S. Fly ash-based adsorbent for adsorption of heavy metals and dyes from aqueous solution: A review. *J. Mater. Res. Technol.* **2021**, *14*, 2751–2774. [CrossRef]

32. Xing, F.; Zheng, X.; Wu, D.; Zhong, H.; Dong, B.; Chen, B.; Fang, G. Study on synergistic solidification method for municipal solid waste incineration fly ash: Core chemical stabilization and shell physical encapsulation. *Case Stud. Constr. Mater.* **2025**, *22*, e04651. [CrossRef]
33. Ali, I.O.; El-Sheikh, S.M.; Salama, T.M.; Bakr, M.F.; Fodial, M.H. Controllable synthesis of NaP zeolite and its application in calcium adsorption. *Sci. China Mater.* **2015**, *58*, 621–633. [CrossRef]

Disclaimer/Publisher's Note: The statements, opinions and data contained in all publications are solely those of the individual author(s) and contributor(s) and not of MDPI and/or the editor(s). MDPI and/or the editor(s) disclaim responsibility for any injury to people or property resulting from any ideas, methods, instructions or products referred to in the content.